

ISOLATION OF ANTIBACTERIAL NANO-HYDROXYAPATITE BIOMATERIAL FROM WASTE BUFFALO BONE AND ITS CHARACTERIZATION

Kshama Parajuli¹, Komal Prasad Malla^{1, 2}, Nicodemus Panchen¹,
Ganga G.C.³, Rameshwar Adhikari^{1, 2, ✉}

<https://doi.org/10.23939/chcht16.01.133>

Abstract. Hydroxyapatite nanoparticles were isolated from a biowaste, buffalo bone, *via* the thermal decomposition method. The resulting white powdered material was characterized by Fourier Transformed Infrared (FTIR) spectroscopy, X-ray Diffraction (XRD), Scanning Electron Microscopy (SEM), and Energy Dispersive X-ray (EDX) analysis. The FTIR spectra confirmed that a heat treatment of the bone powder at the temperature at or above 1223 K removed the organic moieties leading to the formation of a pure inorganic biomineral. The XRD analyses showed that the obtained material was nanocrystalline HAp (nano-HAp) with an average grain diameter of 25 nm, while their rod-shaped particles with their tightly agglomerated morphology were confirmed by the SEM analysis. Besides Calcium (Ca), Phosphorous (P), and Oxygen (O), trace amounts of Aluminum (Al), Magnesium (Mg), Copper (Cu), Zirconium (Zr) and Carbon (C) were also found by EDX analysis. Antibacterial activity of nano-HAp against six standard isolates was investigated by the agar well diffusion method and found to be more susceptible to *Acinetobacter baumannii* while other standard strains such as *Escherichia coli*, *Pseudomonas aeruginosa*, and *Staphylococcus aureus* showed lesser susceptibility and no antibacterial activity was noticed against *Salmonella typhi* and Methicillin resistant *Staphylococcus aureus* (MRSA) with the analysed concentration of nano-HAp suggesting its potential application in biomedical fields.

Keywords: buffalo bone, hydroxyapatite, nanomaterial, antibacterial activity, bioceramic.

1. Introduction

Vertebrate bones mainly consist of about 70 % apatite minerals and about 30 % organic compounds.¹ Hydroxyapatite (HAp), the main inorganic constituent of bones, is considered a biocompatible, osteoconductive, non-inflammatory and safe substance that can make a direct chemical bond with living tissues.^{2,3} Because of the chemical and structural similarities of biological apatite, synthetic HAp has been taken as a promising material for bone substitutes, bone tissue engineering, and coating of metallic implants⁴ as it may protect the implant from the formation of bacterial biofilm and several other applications.⁵⁻⁹ Furthermore, the desired properties of the HAp may be achieved by changing its morphology, porosity, particle size, *etc.* through different ionic substitution into its structure and by choosing suitable synthetic methods.¹⁰

HAp can be conveniently synthesized by various chemical methods such as sol-gel,^{11,12} sonochemical,^{13,14} hydrothermal,^{15,16} using microwave,^{17,18} *etc.* In addition, various biogenic sources such as birds wastes, *e.g.*, eggshells,^{19,20} bones,^{21,22} as well as mammalian bones^{2,15} and fish bones,^{23,24} *etc.* have been used to isolate HAp. Recently, a facile method of synthesizing HAp in an ordinary chemistry laboratory has been featured.²⁵ Furthermore, it has been generally established that bones of different origins lead to a similar yield of HAp in terms of their cost, purity and ease of preparation.²⁶ In fact, biogenic wastes such as animal and bird bones, eggshells, *etc.* offer excellent resources for the preparation of chemical-free and pure HAp.

In the light of the above-mentioned context of the practicability of the HAp and in line with the essence of green chemistry, proper utilization of waste bone for the production of value-added products deem necessary.²⁷ In this regard, waste buffalo bones, which are easily found in a local slaughterhouse, provide an economical resource for the synthesis of HAp. Furthermore, the HAp extracted from bones is considered an important biomaterial since it

¹ Central Department of Chemistry, Tribhuvan University, Kirtipur, Kathmandu, Nepal

² Research Centre for Applied Science and Technology (RECAST), Tribhuvan University, Kirtipur, Kathmandu, Nepal

³ Department of Microbiology, Tri-Chandra M. Campus, Ghantaghar, Kathmandu, Nepal

✉ nepalpolymer@yahoo.com

© Parajuli, K.; Malla, K.P.; Panchen, N.; Ganga G.C., Adhikari, R., 2022

contains a high amount of calcium and phosphorous along with a trace amount of other ions namely Na^+ , Zn^{2+} , Mg^{2+} , K^+ , Si^{2+} , Ba^{2+} , F^- , CO_3^{2-} , etc.²⁸ The extent of such ionic species depends on the age, diet intake, and food habits of the animals.²⁹ The presence of these elements in HAp plays a crucial role in the lifecycle of hard tissue metabolism as well as their antimicrobial activities.^{10,30} Recent studies showed that the HAp particles having a diameter less than 100 nm (nano-HAp) with proper stoichiometry, morphology, and purity have drawn great attention to antimicrobial studies.^{31,32} The antimicrobial properties of nano-HAp can be enhanced by incorporating other metal ions like Ag, Mg, Ni, Zn, Ti, Na, and Ce or Cu into it.⁴

Recently, cerium-substituted HAp synthesized by the sol-gel method was shown to exhibit good antibacterial properties. The Ce^{4+} ions amount in the HAp was found to be an important factor in determining its antibacterial properties similar to silver.³³ The incorporation of Ni^{2+} ions in the HAp structure exhibited inhibitory property in *E. coli* and *S. aureus*.³⁴ It is well known that infectious agents are developing resistance against several antibiotics.^{35,36} Also antibiotics treatments are becoming costly, possess various side effects, and sometimes are not available in varieties.^{36,37} Hence, in the pharmaceutical field, the nano-HAp extracted from natural sources could be used as a drug to replace conventional antibiotics as well as a novel nanosized platform for efficient drug carrier and bone tissue engineering.^{4,38,39} However, only a few such studies have been reported so far.^{4,31,33} Therefore, also as an extension of our recent work concerning the extraction of HAp nano-bioceramic²², the objective of this work has been the extraction of naturally ion-doped nano-HAp from the waste buffalo bone and its characterization for its structure as well as antibacterial properties.

2. Experimental

2.1. Materials and Sample Preparation

The laboratory-grade chemicals required for this research such as acetone ($(\text{CH}_3)_2\text{O}$), ethanol ($\text{C}_2\text{H}_5\text{OH}$), dimethyl sulfoxide (DMSO), sodium hydroxide (NaOH), buffer tablets, etc. were purchased from Fischer Scientific (India) and were used without further purification. For antibacterial activity, nutrient agar, nutrient broth, and Mueller-Hinton agar of HiMedia were used as a nutritional substrate. Distilled water was used for preparing the solutions media and for cleansing purposes.

The femur part of adult buffalo bone was collected from a local slaughterhouse in Kathmandu. The bone marrow present inside the femur bone was removed manually by using forceps and needles. Then it was washed thoroughly first with water and boiled in water for

3 h. The clean fat-free bone was obtained by washing it with acetone several times and drying in a normal oven at 393 K for 48 h. Thus, obtained bones were pulverized to get powder using a laboratory grinder.

2.2. Extraction of HAp

To remove collagen, proteins, fats, and other impurities present in the raw bone powder, reflux assisted alkaline hydrolysis of the bone powder was carried out where the raw bone was treated with 4M aqueous alkali (NaOH) in a ratio of 1:40 (w/v) and heated at 523 K for 5 h. For the constant temperature and homogeneous stirring of the solution, a paraffin liquid oil bath and hot plate with a magnetic stirrer were applied. As obtained deproteinized and defatted bone powder was then washed to neutral pH and heated at 923 K for 5 h in a muffle furnace to obtain bone ash. The bone ash was further calcined at 1223 K and then at 1373 K for 6 h to study the effect of calcination temperature.^{15,40}

2.3. Structural Characterization of Biomaterial

The raw bone powder and bone powder heated at different temperatures were investigated using Fourier Transform Infrared (FTIR) spectroscopy using IRTracer 100 (Shimadzu, Japan) operated in ATR mode. The materials were further analyzed for phase detection and structural characterization by X-ray diffraction (XRD) using monochromatic $\text{Cu K}\alpha$ radiation (D2 Phaser Diffractometer, Bruker, Germany). The average crystallite size was calculated from the XRD data applying Debye-Scherrer's equation.²²

$$D = \frac{K\lambda}{\beta \cos\theta} \quad (1)$$

where D is the average crystallite size, K the broadening constant, λ the wavelength of $\text{Cu K}\alpha$ radiation (0.15406 nm), β the full-width at half maximum (FWHM) in radians, θ is the diffraction angle in degrees.

Surface morphological analysis of the prepared sample was carried out by using a field emission gun scanning electron microscope (FE-SEM, Hitachi, S-7400). The estimation of calcium and phosphorus (Ca/P) elemental ratio was performed with the help of an energy dispersive X-ray spectrometer (EDX-8000, Shimadzu, Japan).

2.4. Bacterial Culture

Pathogenic reference bacterial strains, namely, gram-negative (*Escherichia coli* (ATCC 25922), *Pseudomonas aeruginosa* (ATCC 27853)), gram-positive (*Staphylococcus aureus* (ATCC 29213)), clinical isolates gram-negative (*Acinetobacter baumannii*, *Salmonella*

typhi) and clinical isolates gram-positive (Methicillin resistant *Staphylococcus aureus* (MRSA)) were collected from the Central Department of Microbiology, Kirtipur, Kathmandu Nepal.

2.5. Antibacterial Activity Assessment

The antibacterial properties of the HAp were analyzed by the diffusion method using sterile Mueller-Hinton agar (MHA) using a standard protocol.^{41,42} Fresh culture of the American Type Culture Collection (ATCC) reference bacterial strains ((quality control strains for antimicrobial susceptibility testing), namely, gram-negative (*Escherichia coli* (ATCC 25922), *Pseudomonas aeruginosa* (ATCC 27853)), gram-positive (*Staphylococcus aureus* (ATCC 29213)), the identified clinical isolates such as gram-negative (*Acinetobacter baumannii*, *Salmonella typhi*) and gram-positive (Methicillin-resistant *Staphylococcus aureus* (MRSA)) were cultured in nutrient agar at 310 K for 24 h. Fresh cultures of these isolates were sub-cultured in nutrient broth (NB) for 3–4 h at 310 K to obtain the turbidity of 0.5 McFarland standard which is equivalent to $1.5 \cdot 10^8$ bacterial suspension/mL as an inoculum. The organisms were lawn cultured with the help of sterile cotton swabs in MHA agar. Then with the help of a sterile 5 mm cork-borer, wells were made in the MHA. The HAp suspensions of various concentrations (5, 10, 20, 30, and 50 mg/mL) were prepared by dissolving the respective powder in dimethyl sulfoxide (DMSO). Wells were filled with 50 μ L HAp of different concentrations with the help of a micropipette. DMSO was taken as a negative control. After complete diffusion, the plates were carefully placed in an incubator and maintained at 310 K for 24 h. The next day, the zone of inhibition (ZOI) was noted.

3. Results and Discussion

3.1. Structure and Morphology of HAp

The comparison of the FTIR spectra of raw and alkali-treated bone powder samples calcined at 1223 K and 1373 K is shown in Fig. 1. The possible functional groups and their modes of vibration according to the peaks that appeared in FTIR spectra are summarized in Table 1.

Distinct bands due to the presence of phosphate groups (in the region of 1200–900 and 620–500 cm^{-1})⁴³, hydroxide group (small bands in the region of 3670–3570 and 640–625 cm^{-1})⁴⁴ and carbonate group (small band in the region of 1400–1600 and 870–880 cm^{-1})⁴⁵ are observed in all type of samples. The observed results are in agreement with those reported in earlier investigations.^{3,15,45} However, in the case of raw bone powder, phosphate, hydroxide and carbonate bands are

not visible, which could be due to various organic-inorganic cross-linked structures present in the raw bone powder. The observed results are in agreement with previous studies.^{15,46} Furthermore, the bands around 1646 and 1241 cm^{-1} appear only in a raw bone powder attributed to the organic compounds present in it.^{3,46,47}

In the case of alkali-treated bone powder, only a few absorption bands appeared whereas when alkali-treated bone powder calcined at 1223 K and 1373 K showed broad absorption bands. The observed bands nearly match with the bands of the HAp spectrum reported in the literature.^{3,48} The peaks located around 3560 and 639 cm^{-1} can be attributed to the stretching and liberation vibration of (OH) group, respectively.⁴⁹

The IR bands located at 1084, 1034, 963 599, 561 and 472 cm^{-1} are due to the vibrations of PO_4^{3-} groups. Among these bands, the band positioned at 963 cm^{-1} is assigned to the symmetric stretching mode $\nu_1(\text{PO}_4^{3-})$ ²¹ while the peaks located at 1084 and 1034 cm^{-1} correspond to the asymmetric stretching mode $\nu_3(\text{PO}_4^{3-})$.⁵⁰ Likewise, the peaks centred at 599 and 561 cm^{-1} correspond to asymmetric bending modes $\nu_4(\text{PO}_4^{3-})$ and the peak at 472 cm^{-1} corresponds to the symmetric bending mode of $\nu_2(\text{PO}_4^{3-})$.⁵¹ In addition weak intensity bands located around 2160 and 2043 cm^{-1} can be assigned to the overtone and combination of ν_3 and ν_1 mode of PO_4^{3-} group.^{3,51}

The double bands centred at 1449 and 1417 cm^{-1} along with the single band centred at 875 cm^{-1} are due to CO_3^{2-} ions.^{43,47} This is an indication of a minor amount of CO_3^{2-} incorporation in the apatite structure constituting the bone mineral.^{47,52} The presence of CO_3^{2-} may play a vital role in enhancing its medicinal properties as carbonate-substituted natural HAp was found to be better for bio-resorbable bone substitutes.^{30,53} However, the intensity of such bands gradually decreases when the high-temperature calcination process is applied⁵¹ indicating more and more loss of carbon content of bone powder at 1373 K.

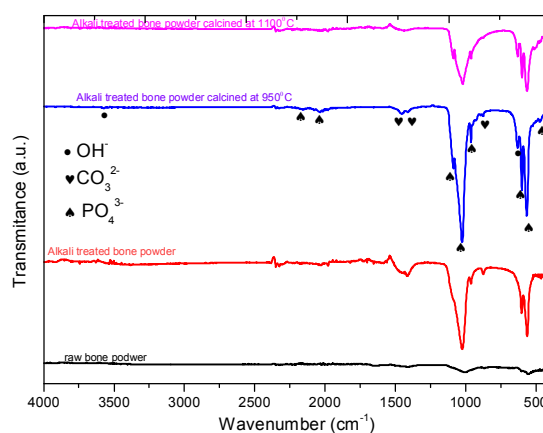


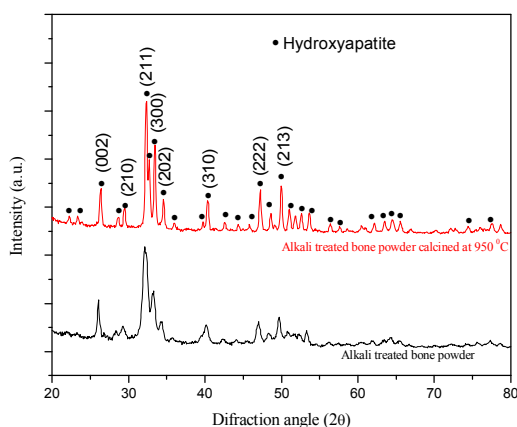
Fig. 1. FTIR spectra of raw, alkali-treated, and calcined (at 1223 K and 1373 K after alkali treatment) bone powder

Table 1. Summary of the functional groups and modes of vibration of various peaks of raw, alkali-treated, and calcined (at 1223 K and 1373 K after alkali treatment) bone samples obtained from FTIR spectra

Functional groups and mode of vibration	Raw bone powder, cm ⁻¹	Alkali treated, cm ⁻¹	Calcined at 1223 K, cm ⁻¹	Calcined at 1373 K, cm ⁻¹
OH (stretching)	3287	3460	3570	3574
OH (liberation)	-	-	639	635
(PO ₄ ³⁻) (stretching)	1007	1030, 969	1084, 1026, 963	1090, 1030, 969
(PO ₄ ³⁻) (bending)	607, 554	608, 558	598, 561, 475	594, 564
CO ₃ ²⁻ (stretching)	1407	1417	1459, 1408	-
CO ₃ ²⁻ (bending)	874	872	872	-

There are no absorption bands that correspond to organic impurities (N–H and C–H band)⁵⁴ for the alkali-treated bone powder calcined at 1223 K and 1373 K suggesting that the extracted HAp would be free from organic impurities.²⁷ Furthermore, an increase in the sharpness of bands, especially that of 639, 599 and 561 cm⁻¹ band, suggests a well-crystallized HAp.⁵¹ Hence, as-prepared bone powder proved to be crystalline HAp and found the best to be formed when calcined at 1223 K after alkaline treatment as evidenced by the presence of the expected FTIR peaks in this sample.

The phase structure of the isolated HAp was studied by X-ray diffraction and the observed results for an alkali-treated raw bone sample, as well as a calcined alkali-treated bone powder at 1223 K acquired from 2 θ values ranging from 20° to 80° are shown in Fig. 2.

**Fig. 2.** XRD pattern of only alkali-treated and the calcined bone powder at 1223 K

The degrees of sharpness of the peaks were found to increase gradually on raising the heat treatment temperature informing the increase in crystallinity of the extracted material as the calcination process helps to release the collagens, fats and other impurities that are bound to the bone powders.⁵⁵

The results are in line with the former studies reports.^{30,47} Furthermore, the broad diffraction peaks observed are closely matched to the stoichiometric HAp

characterized pattern (based on ICDD 9-432). The slight deviation of the diffraction peaks from standard peaks could be due to metal ions (Na⁺, Mg²⁺, Al³⁺, Cu²⁺, Zr²⁺ etc.) present naturally in the crystal lattice of HAp.^{22,56}

Among these, some intense peaks are observed at 2 θ values of 26.44°, 29.52°, 32.26°, 33.29°, 34.49°, 40.31°, 47.16° and 50.07° which correspond to Miller planes (022), (210), (211), (300), (202), (310), (222), and (213), etc.^{29,51} Thus, the bone powder calcined at 1223 K after alkali treatment contains pure HAp phase and the obtained result is comparable with the previously reported result.⁵⁴ In addition, the average grain size of the HAp was found to be 25 nm using the Debye-Scherrer equation and hence it could be considered as naturally ion-doped nano-HAp.

The morphology of the HAp obtained after heat treatment of the alkali-treated bone sample at 1223 K is shown in Fig. 3. As can be seen from the SEM images the as-obtained HAp nanoparticles contained a mixture of differently sized rod-shaped crystalline textures with agglomeration which might have been formed due to their high surface energy and the SEM image is comparable with literature images.^{16,57} The width of the platelets as observed in Fig. 3. is in the range of 100–300 nm, which is far from that observed by XRD (25 nm) due to agglomeration.

Table 2 and Fig. 4. show the elemental composition and EDX spectrum of isolated HAp from alkali-treated bone powder calcined at 1223 K. The powder was found to consist of Ca, P, O, along with a small amount of Al, Mg, Cu, Zr and C. These trace elements make as-obtained HAp as ion-doped HAp and are essential for antimicrobial activity as well as bone growth.^{17,58} This analysis showed that the HAp obtained after thermal treatment at 1223 K has mostly inorganic phases. Furthermore, the calcium to the phosphorous elemental ratio of the HAp from EDX study was found to be 1.605, which is smaller (*i.e.*, Ca-deficient) compared to an ideal stoichiometric ratio (1.67).^{51,54} However, the obtained Ca/P ratio was closed to literature data where the Ca/P ratio was reported to be 1.66 and 1.603 for the HAp recovered from a bovine bone⁵⁹ and pig bone,² respectively. Similarly, in another study, the ratio of calcium to phosphorous was reported to

be 1.86 for the HAp extracted from bovine bone,¹⁵ which is higher than that in the stoichiometric material. These discrepancies in the Ca/P elemental ratio of biogenic HAp

may be due to different biogenic sources (bone) of HAp as the trace elemental composition in bone depends on the diet intake and age of the animal itself.^{28,29}

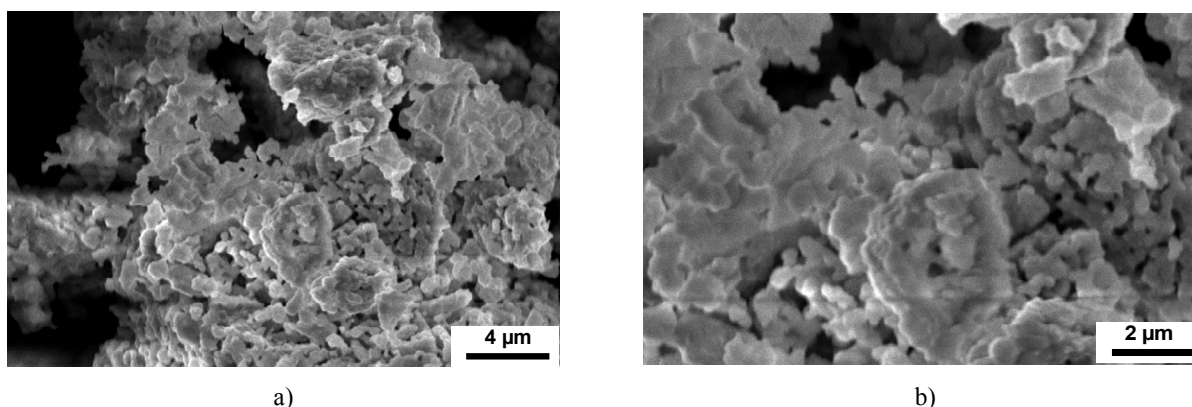


Fig. 3. Lower (a) and higher (b) magnified SEM images of the HAp powder obtained after alkali treatment followed by calcination of bone powder at 1223 K

Table 2. Elemental composition of HAp obtained from bone powder calcined at 1223 K determined by EDX analysis

Element	Weight %	Atomic %	Element	Weight %	Atomic %	Element	Weight %	Atomic %
C	3.79	7.78	Mg	0.13	0.13	Ca	44.61	27.41
O	12.5	55.85	Al	0.02	0.02	Cu	0.30	0.12
Na	0.60	0.64	P	27.78	6.36	Zr	2.27	1.69

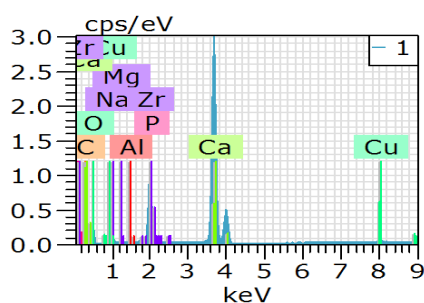


Fig. 4. EDX spectra of the HAp obtained by heat treatment of the alkali-treated bone powder at 1223 K

3.2. Antimicrobial Properties of Nano-HAp

The antibacterial activity of isolated HAp was investigated by using human pathogenic bacteria, namely *Acinetobacter baumannii*, *Salmonella typhi*, Methicillin-resistant *Staphylococcus aureus* (MRSA), *Escherichia coli*, *Pseudomonas aeruginosa*, and *Staphylococcus aureus* by the agar well diffusion method. The observed zones of inhibition (ZOI) after 24 h of incubation are indexed in Table 3.

Among the 6 isolates, the nano-HAp was seen more effective against *Acinetobacter baumannii*, which produced ZOI of diameter 16 mm at 30 mg/mL, 14 mm at

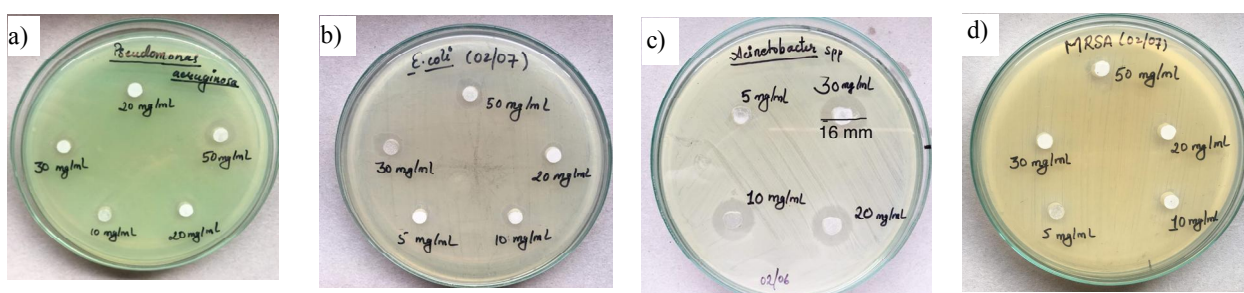
10 mg/mL and 20 mg/mL of nano-HAp, respectively. Other standard strains such as *Escherichia coli*, *Pseudomonas aeruginosa* and *Staphylococcus aureus* produced ZOI diameters of 11, 10, and 9 mm, respectively, only at higher concentrations of nano-HAp, i.e., 50 mg/mL, and below 30 mg/mL of nano-HAp did not show antibacterial activity (no ZOI observed), as shown in Table 1 and Fig. 5. Furthermore, no ZOI was noticed against *Salmonella typhi* and MRSA with the analysed concentration of nano-HAp. A similar result was reported by Balu *et al.*,⁶ the susceptibility to *E. coli* and *S. aureus* was studied and ZOI was found to be 13 and 14.5 mm, respectively, at 50 mg/mL of nano-HAp synthesized from cuttlefish bone. Resmim *et al.*³⁵ showed a growth inhibitory effect of *S. aureus* up to 81% and 56% by using nano-HAp from the bovine and porcine bone obtained by calcination at 1273 K, respectively.

Although various properties of HAp including antibacterial properties depend on the size, surface area, morphology, porosity, crystallinity, stoichiometry, and types and concentration of ions present in it^{6,10,35}, many of the researches reported that the antibacterial activity of nano-HAp is enhanced by doping with other elements like Zn, Cu, Ag, Co, Ce, Se, *etc.*^{10,30,40,60} Hence different ions and its concentration present in the nano-HAp may play a crucial role in inhibiting the bacterial growth^{32,33} along with other properties such as morphology, size, *etc.*⁶

Table 3. Zone of inhibition formed by nano-HAp on quality control strains and clinically isolated bacterial strains subjected to interaction with different bacteria as indicated

Tested bacteria	Gram reaction	ZOI (mm) DMSO (-ve control)	ZOI (mm) of nano-HAp at different concentrations (mg/mL)				
			5	10	20	30	50
<i>Pseudomonas aeruginosa</i> (ATCC 27853)	-ve	-	-	-	-	-	10
<i>Escherichia coli</i> (ATCC 25922)	-ve	-	-	-	-	slightly	11
<i>Acinetobacter baumannii</i>	-ve	-	-	14	14	16	-
<i>Salmonella typhi</i>	-ve	-	-	-	-	-	-
<i>Staphylococcus aureus</i> (ATCC 29213)	+ve	-	-	-	-	8	9
MRSA	+ve	-	-	-	-	-	-

Note: -ve means gram-negative, +ve means gram-positive and '-' means no zone of inhibition

**Fig. 5.** Photographs of antibacterial test results of nano-HAp: *Pseudomonas aeruginosa* (a), *Escherichia coli* (b), *Acinetobacter baumannii* (c) and Methicillin-resistant *Staphylococcus aureus* (MRSA) (d)

Moreover, due to the electrostatic attraction between negatively charged bacterial surface and positively charged HAp³⁸, different ions present in the HAp may release in the surrounding environment, which might cause precipitation and coagulation of proteins and enzymes present in the bacterial cell as a result, structural damage occurred within the cell wall and bacterial membranes which ultimately leads to the death of the cell and hence microbes.^{11,17,61} Such germicidal property of metals ions, especially heavy metal ions, is known as an oligodynamic effect.⁶² In addition, the different susceptibility of the material to microbial targets is probably due to differences in the microbial cell wall structures.³⁸ The results indicate that the nano-HAp extracted from biological sources may be further useful to combat bacterial infections by encapsulation of antibiotics following the principle of targeted drug delivery.

4. Conclusions

Alkaline hydrolysis followed by a calcination process was applied to isolate the nano-HAp from waste buffalo bone. This method is cost-effective and environmentally friendly for the isolation of nanoscale biomaterials.

The alkaline hydrolysis and calcination at 1223 K removed the organic impurities from the mineral matrix confirming the formation of carbonate-substituted crystalline HAp as suggested by the IR peaks corresponding to PO_4^{3-} , OH^- and CO_3^{2-} . XRD study revealed that the isolated biomineral was the nanocrystalline HAp.

The presence of Ca, P and O as major elements and Cu, Zr, Na, Mg, Al, and C as trace elements was confirmed by EDX analysis of the nano-HAp. The Ca/P elemental ratio was found to be 1.605, smaller than the ideal stoichiometric value of HAp, which might have been caused by the ion-doping nature of the HAp derived from biogenic sources.

The nano-HAp biomaterial extracted from the bone was found to possess the rod-shaped agglomerated structure as shown by electron microscopic studies.

Among the six standard different isolates investigated for antibacterial activity, nano-HAp was found to be more susceptible to *Acinetobacter baumannii* while other standard strains such as *Escherichia coli*, *Pseudomonas aeruginosa* and *Staphylococcus aureus* showed lesser susceptibility at the applied concentrations of nano-HAp and no antibacterial activity was noticed against *Salmonella typhi* and MRSA.

The observed antibacterial properties of the isolated nanocrystalline HAp could be attributed to the ion-doped nature of the HAp. Thus, natural ion-doped bioceramic obtained from biogenic sources has the potential to be applied in different biomedical fields including orthopaedic, dental, and implant applications.

Acknowledgements

The authors would like to acknowledge the University Grants Commission (UGC), Sanathimi, Bhaktapur, Nepal, for providing financial support (SRDI-75/76-S&T-4). We further thank Dr. Bipin Dahal, Department of BIN Convergence Technology, Chonbuk National University, Jeonju, the Republic of Korea for SEM images.

References

- [1] Manalu, J.L.; Soegijono, B.; Indrani, D.J. Characterization of Hydroxyapatite Derived from Bovine Bone. *Asian J. Appl. Sci.* **2015**, *3* (4), 758–765.
- [2] Lim, K.T.; Kim, J.W.; Kim, J.; Chung, J.H. Development and Evaluation of Natural Hydroxyapatite Ceramics Produced by the Heat Treatment of Pig Bones. *J. Biosyst. Eng.* **2014**, *39*, 227–234. <https://doi.org/10.5307/jbe.2014.39.3.227>
- [3] Ooi, C.Y.; Hamdi, M.; Ramesh, S. Properties of Hydroxyapatite Produced by Annealing of Bovine Bone. *Ceram. Int.* **2007**, *33*, 1171–1177. <https://doi.org/10.1016/j.ceramint.2006.04.001>
- [4] Kolmas, J.; Groszyk, E.; Kwiatkowska, R.D. Substituted Hydroxyapatites with Antibacterial Properties. *Biomed Res. Int.* **2014**, *2014*, Article ID 178123. <https://doi.org/10.1155/2014/178123>
- [5] Rana, M.; Akhtar, N.; Rahman, S.; Hasan, Z. Extraction and Characterization of Hydroxyapatite from Bovine Cortical Bone and Effect of Radiation. *Int. J. Biosci.* **2017**, *11*, 20–30. <https://doi.org/10.12692/ijb/11.3.20-30>
- [6] Balu, S.; Sundaradoss, M. V.; Andra, S.; Jeevanandam, J. Facile Biogenic Fabrication of Hydroxyapatite Nanorods Using Cuttlefish Bone and Their Bactericidal and Biocompatibility Study. *Beilstein J. Nanotechnol.* **2020**, *11*, 285–295. <https://doi.org/10.3762/bjnano.11.21>
- [7] Savvova, O. Biocide Apatite Glass-Ceramic Materials for Bone Endoprosthetics. *Chem. Chem. Technol.* **2013**, *7*, 109–112. <https://doi.org/10.23939/chcht07.01.109>
- [8] Savvova, O.; Babich, O.; Fesenko, O. Investigation of Structure Formation in Calciumsilicophosphate Glass-Ceramic Coatings for Dental Implants. *Chem. Chem. Technol.* **2018**, *12*, 244–250. <https://doi.org/10.23939/chcht12.02.244>
- [9] Nur, A.; Budiman, A. W.; Jumari, A.; Nazriati, N.; Fajaroh.; F. Electrosynthesis of Ni-Co/Hydroxyapatite As a Catalyst for Hydrogen Generation via the Hydrolysis of Aqueous Sodium Borohydride [NaBH₄] Solutions. *Chem. Chem. Technol.* **2021**, *15*, 389–394. <https://doi.org/10.23939/chcht15.03.389>
- [10] Singh, G.; Singh, R.P.; Jolly, S.S. Customized Hydroxyapatites for Bone-Tissue Engineering and Drug Delivery Applications: A Review. *J. Sol-Gel Sci. Technol.* **2020**, *94*, 505–530. <https://doi.org/10.1007/s10971-020-05222-1>
- [11] Fathi, M.H.; Hanifi, A.; Mortazavi, V. Preparation and Bioactivity Evaluation of Bone-like Hydroxyapatite Nanopowder. *J. Mater. Process. Technol.* **2008**, *202* (1-3), 536–542. <https://doi.org/10.1016/j.jmatprotec.2007.10.004>
- [12] Eshtiagh-Hosseini, H.; Housaindokht, M.R.; Chahkandi, M. Effects of Parameters of Sol-Gel Process on the Phase Evolution of Sol-Gel-Derived Hydroxyapatite. *Mater. Chem. Phys.* **2007**, *106* (2–3), 310–316. <https://doi.org/10.1016/j.matchemphys.2007.06.002>
- [13] Han, Y.C.; Wang, X.Y.; Li, S.P. Change of Phase Composition and Morphology of Sonochemically Synthesised Hydroxyapatite Nanoparticles with Glycosaminoglycans during Thermal Treatment. *Adv. Appl. Ceram.* **2009**, *108*, 400–405. <https://doi.org/10.1179/174367609X414134>
- [14] Giardina, M.A.; Fanovich, M.A. Synthesis of Nanocrystalline Hydroxyapatite from Ca[OH]₂ and H₃PO₄ Assisted by Ultrasonic Irradiation. *Ceram. Int.* **2010**, *36*, 1961–1969. <https://doi.org/10.1016/j.ceramint.2010.05.008>
- [15] Barakat, N.A.M.; Khil, M.S.; Omran, A.M.; Sheikh, F.A.; Kim, H.Y. Extraction of Pure Natural Hydroxyapatite from the Bovine Bones Bio Waste by Three Different Methods. *J. Mater. Process. Technol.* **2009**, *209* (7), 3408–3415. <https://doi.org/10.1016/j.jmatprotec.2008.07.040>
- [16] Neira, I.S.; Guitián, F.; Taniguchi, T.; Watanabe, T.; Yoshimura, M. Hydrothermal Synthesis of Hydroxyapatite Whiskers with Sharp Faceted Hexagonal Morphology. *J. Mater. Sci.* **2008**, *43* (7), 2171–2178. <https://doi.org/10.1007/s10853-007-2032-9>
- [17] Iqbal, N.; Abdul Kadir, M.R.; Nik Malek, N.A.N.; Humaimi Mahmood, N.; Raman Murali, M.; Kamarul, T. Rapid Microwave Assisted Synthesis and Characterization of Nanosized Silver-Doped Hydroxyapatite with Antibacterial Properties. *Mater. Lett.* **2012**, *89*, 118–122. <https://doi.org/10.1016/j.matlet.2012.08.057>
- [18] Hassan, M.N.; Mahmoud, M.M.; El-Fattah, A.A.; Kandil, S. Microwave-Assisted Preparation of Nano-Hydroxyapatite for Bone Substitutes. *Ceram. Int.* **2016**, *42* (3), 3725–3744. <https://doi.org/10.1016/j.ceramint.2015.11.044>
- [19] Ronan, K.; Kannan, M.B. Novel Sustainable Route for Synthesis of Hydroxyapatite Biomaterial from Biowastes. *ACS Sustain. Chem. Eng.* **2017**, *5* (3), 2237–2245. <https://doi.org/10.1021/acssuschemeng.6b02515>
- [20] Abdulrahman, I.; Tijani, H.I.; Mohammed, B.A.; Saidu, H.; Yusuf, H.; Ndejiko Jibrin, M.; Mohammed, S. From Garbage to Biomaterials: An Overview on Egg Shell Based Hydroxyapatite. *J. Mater.* **2014**, *2014*, Article ID 802467. <https://doi.org/10.1155/2014/802467>
- [21] Rajesh, R.; Hariharasubramanian, A.; Ravichandran, Y.D. Chicken Bone as a Bioresource for the Bioceramic [Hydroxyapatite]. *Phosphorus, Sulfur Silicon Relat. Elem.* **2012**, *187* (8), 914–925. <https://doi.org/10.1080/10426507.2011.650806>
- [22] Malla, K.P.; Regmi, S.; Nepal, A.; Bhattarai, S.; Yadav, R. J.; Sakurai, S.; Adhikari, R. Extraction and Characterization of Novel Natural Hydroxyapatite Bioceramic by Thermal Decomposition of Waste Ostrich Bone. *Int. J. Biomater.* **2020**, *2020*, Article ID 1690178. <https://doi.org/10.1155/2020/1690178>
- [23] Fara, A.N.K.A.; Abdullah, H.Z. Characterization of Derived Natural Hydroxyapatite [HAp] Obtained from Different Types of Tilapia Fish Bones and Scales. *AIP Conf. Proc.* **2015**, *1669*, 020071–0200776. <https://doi.org/10.1063/1.4919215>
- [24] Venkatesan, J.; Lowe, B.; Manivasagan, P.; Kang, K.H.; Chalisserry, E.P.; Anil, S.; Kim, D.G.; Kim, S.K. Isolation and Characterization of Nano-Hydroxyapatite from Salmon Fish Bone. *Materials* **2015**, *8* (8), 5426–5439. <https://doi.org/10.3390/ma8085253>
- [25] Pandey, G.; Dhakal, K.N.; Singh, A.K.; Dhungel, S.K.; Adhikari, R. Facile Methods of Preparing Pure Hydroxyapatite

- Nanoparticles in Ordinary Laboratories. *Bibechana* **2021**, *18* (1), 83–90. <https://doi.org/10.3126/bibechana.v18i1.29600>
- [26] Laonapakul, T. Synthesis of Hydroxyapatite from Biogenic Wastes. *KKU Eng. J.* **2015**, *42* (3), 269–275. <https://doi.org/10.14456/kkuenj.2015.30>
- [27] Odusote, J.K.; Danyuo, Y.; Baruwa, A.D.; Azeez, A.A. Synthesis and Characterization of Hydroxyapatite from Bovine Bone for Production of Dental Implants. *J. Appl. Biomater. Funct. Mater.* **2019**, *17*, 1–7. <https://doi.org/10.1177/2280800019836829>
- [28] Mohd Pu'ad, N.A.S.; Koshy, P.; Abdullah, H.Z.; Idris, M.I.; Lee, T.C. Syntheses of Hydroxyapatite from Natural Sources. *Heliyon* **2019**, *5*, 1–14. <https://doi.org/10.1016/j.heliyon.2019.e01588>
- [29] Ramesh, S.; Loo, Z.Z.; Tan, C.Y.; Chew, W.J.K.; Ching, Y.C.; Tarlochan, F.; Chandran, H.; Krishnasamy, S.; Bang, L.T.; Sarhan, A.A.D. Characterization of Biogenic Hydroxyapatite Derived from Animal Bones for Biomedical Applications. *Ceram. Int.* **2018**, *44* (9), 10525–10530. <https://doi.org/10.1016/j.ceramint.2018.03.072>
- [30] Uskoković, V.; Iyer, M.A.; Wu, V.M. One Ion to Rule Them All: The Combined Antibacterial, Osteoinductive and Anticancer Properties of Selenite-Incorporated Hydroxyapatite. *J. Mater. Chem. B.* **2017**, *5* (7), 1430–1445. <https://doi.org/10.1039/c6tb03387c>
- [31] Zhang, X.; Chaimayo, W.; Yang, C.; Yao, J.; Miller, B.L.; Yates, M.Z. Silver-Hydroxyapatite Composite Coatings with Enhanced Antimicrobial Activities through Heat Treatment. *Surf. Coatings Technol.* **2017**, *325*, 39–45. <https://doi.org/10.1016/j.surfcoat.2017.06.013>
- [32] Ajduković, Z.R.; Mihajilov-Krstev, T.M.; Ignjatović, N.L.; Stojanović, Z.; Mladenović-Antić, S.B.; Kocić, B.D.; Najman, S.; Petrović, N.D.; Uskoković, D.P. In Vitro Evaluation of Nanoscale Hydroxyapatite-Based Bone Reconstructive Materials with Antimicrobial Properties. *J. Nanosci. Nanotechnol.* **2016**, *16*, 1420–1428. <https://doi.org/10.1166/jnn.2016.10699>
- [33] Padmanabhan, V.P.; Kulandaivelu, R.; Nellaippan, S.N.T.S.; Lakshmiopathy, M.; Sagadevan, S.; Johan, M.R. Facile Fabrication of Phase Transformed Cerium[IV] Doped Hydroxyapatite for Biomedical Applications – A Health Care Approach. *Ceram. Int.* **2020**, *46*, 2510–2522. <https://doi.org/10.1016/j.ceramint.2019.09.245>
- [34] Jenifer, A.; Sakthivel, P.; Senthilarasan, K.; Sivaprakash, P.; Arumugam, S. In Vitro Analysis of Nickel Doped Hydroxyapatite for Biomedical Applications. *Int. J. Sci. Technol. Res.* **2019**, *8* (11), 781–787.
- [35] Resmim, C.M.; Dalpasquale, M.; Vielmo, N.I.C.; Mariani, F.Q.; Villalba, J.C.; Anaissi, F.J.; Caetano, M.M.; Tusi, M.M. Study of Physico-Chemical Properties and in Vitro Antimicrobial Activity of Hydroxyapatites Obtained from Bone Calcination. *Prog. Biomater.* **2019**, *8*, 1–9. <https://doi.org/10.1007/s40204-018-0105-2>
- [36] Wang, L.; Hu, C.; Shao, L. The Antimicrobial Activity of Nanoparticles: Present Situation and Prospects for the Future. *Int. J. Nanomedicine* **2017**, *12*, 1227–1249. <https://doi.org/10.2147/IJN.S121956>
- [37] Shrestha, P.; Cooper, B.S.; Coast, J.; Opong, R.; Do Thi Thuy, N.; Phodha, T.; Celhay, O.; Guerin, P.J.; Wertheim, H.; Lubell, Y. Enumerating the Economic Cost of Antimicrobial Resistance per Antibiotic Consumed to Inform the Evaluation of Interventions Affecting Their Use. *Antimicrob. Resist. Infect. Control* **2018**, *7*, Article number 98. <https://doi.org/10.1186/s13756-018-0384-3>
- [38] Ciobanu, C.S.; Iconaru, S.L.; Chifiriuc, M.C.; Costescu, A.; Le Coustumer, P.; Predoi, D. Synthesis and Antimicrobial Activity of Silver-Doped Hydroxyapatite Nanoparticles. *Biomed Res. Int.* **2013**, *2013*, Article ID 916218. <https://doi.org/10.1155/2013/916218>
- [39] Swetha, M.; Sahithi, K.; Moorthi, A.; Saranya, N.; Saravanan, S.; Ramasamy, K.; Srinivasan, N.; Selvamurugan, N. Synthesis, Characterization, and Antimicrobial Activity of Nano-Hydroxyapatite-Zinc for Bone Tissue Engineering Applications. *J. Nanosci. Nanotechnol.* **2012**, *12*, 167–172. <https://doi.org/10.1166/jnn.2012.5142>
- [40] Venkatesan, J.; Kim, S.K. Effect of Temperature on Isolation and Characterization of Hydroxyapatite from Tuna [Thunnus Obesus] Bone. *Materials* **2010**, *3*, 4761–4772. <https://doi.org/10.3390/ma3104761>
- [41] Magaldi, S.; Mata-Essayag, S.; Hartung De Capriles, C.; Perez, C.; Colella, M. T.; Olaizola, C.; Ontiveros, Y. Well Diffusion for Antifungal Susceptibility Testing. *Int. J. Infect. Dis.* **2004**, *8*, 39–45. <https://doi.org/10.1016/j.ijid.2003.03.002>
- [42] Balouiri, M.; Sadiki, M.; Ibsouda, S.K. Methods for in Vitro Evaluating Antimicrobial Activity: A Review. *J. Pharm. Anal.* **2016**, *6* (2), 71–79. <https://doi.org/10.1016/j.jpaha.2015.11.005>
- [43] Poralan, G.M.; Gambe, J.E.; Alcantara, E.M.; Vequizo, R.M. X-Ray Diffraction and Infrared Spectroscopy Analyses on the Crystallinity of Engineered Biological Hydroxyapatite for Medical Application. *IOP Conf. Ser. Mater. Sci. Eng.* **2015**, *79*, 1–7. <https://doi.org/10.1088/1757-899X/79/1/012028>
- [44] Sobczak-Kupiec, A.; Wzorek, Z. The Influence of Calcination Parameters on Free Calcium Oxide Content in Natural Hydroxyapatite. *Ceram. Int.* **2012**, *38*, 641–647. <https://doi.org/10.1016/j.ceramint.2011.06.065>
- [45] Fleet, M.E. Infrared Spectra of Carbonate Apatites: Evidence for a Connection between Bone Mineral and Body Fluids. *Am. Mineral.* **2017**, *102*, 149–157. <https://doi.org/10.2138/am-2017-5704>
- [46] Khoo, W.; Nor, F.M.; Ardhyananta, H.; Kurmiawan, D. Preparation of Natural Hydroxyapatite from Bovine Femur Bones Using Calcination at Various Temperatures. *Procedia Manuf.* **2015**, *2*, 196–201. <https://doi.org/10.1016/j.promfg.2015.07.034>
- [47] Bahrololoom, M.E.; Javidi, M.; Javadpour, S.; Ma, J. Characterisation of Natural Hydroxyapatite Extracted from Bovine Cortical Bone Ash. *J. Ceram. Process. Res.* **2009**, *10* (2), 129–138. <https://doi.org/10.36410/jcpr.2009.10.2.129>
- [48] Ofudje, E.A.; Rajendran, A.; Adeogun, A.I.; Idowu, M.A.; Kareem, S.O.; Pattanayak, D.K. Synthesis of Organic Derived Hydroxyapatite Scaffold from Pig Bone Waste for Tissue Engineering Applications. *Adv. Powder Technol.* **2018**, *29*, 1–8. <https://doi.org/10.1016/j.apt.2017.09.008>
- [49] Liu, P.; Li, Z.; Yuan, L.; Sun, X.; Zhou, Y. Pourbaix-Guided Mineralization and Site-Selective Photoluminescence Properties of Rare Earth Substituted B-Type Carbonated Hydroxyapatite Nanocrystals. *Molecules* **2021**, *26* (3), 540. <https://doi.org/10.3390/molecules26030540>
- [50] Sofronia, A.M.; Baies, R.; Anghel, E.M.; Marinescu, C.A.; Tanasescu, S. Thermal and Structural Characterization of Synthetic and Natural Nanocrystalline Hydroxyapatite. *Mater. Sci. Eng. C.* **2014**, *43*, 153–163. <https://doi.org/10.1016/j.msec.2014.07.023>
- [51] Markovic, M. Preparation and Comprehensive Characterization of a Calcium Hydroxyapatite Reference Material Volume. *J. Res. Natl. Inst. Stand. Technol.* **2004**, *109*, 253–568. <https://doi.org/10.1097/00000658-199102000-00001>
- [52] Walters, M.A.; Leung, Y.C.; Blumenthal, N.C.; Konsker, K.A.; LeGeros, R.Z. A Raman and Infrared Spectroscopic Investigation of Biological Hydroxyapatite. *J. Inorg. Biochem.* **1990**, *39* (3), 193–200. [https://doi.org/10.1016/0162-0134\(90\)84002-7](https://doi.org/10.1016/0162-0134(90)84002-7)
- [53] Jaber, H.L.; Hammood, A.S.; Parvin, N. Synthesis and Characterization of Hydroxyapatite Powder from Natural Camelus Bone. *J. Aust. Ceram. Soc.* **2018**, *54*, 1–10. <https://doi.org/10.1007/s41779-017-0120-0>
- [54] Esmailkhanian, A.; Shariifanji, F.; Abouchenari, A.; Rouhani, A.; Parvin, N.; Irani, M. Synthesis and Characterization of Natural Nano-Hydroxyapatite Derived from Turkey Femur-Bone Waste. *Appl. Biochem. Biotechnol.* **2019**, *189*, 919–932. <https://doi.org/10.1007/s12010-019-03046-6>

- [55] Hariani, P.L.; Muryati, M.; Said, M.; Salni, S. Synthesis of Nano-Hydroxyapatite from Snakehead [Channa Striata] Fish Bone and Its Antibacterial Properties. *Key Eng. Mater.* **2020**, *840*, 293–299. <https://doi.org/10.4028/www.scientific.net/kem.840.293>
- [56] Bano, N.; Jikan, S.S.; Basri, H.; Adzila, S.; Zago, D.M. XRD and FTIR Study of A&B Type Carbonated Hydroxyapatite Extracted from Bovine Bone. *AIP Conf. Proc.* **2019**, *2068*, 0201001-0201006. <https://doi.org/10.1063/1.5089399>
- [57] Shavandi, A.; Bekhit, A.E.D.A.; Ali, A.; Sun, Z. Synthesis of Nano-Hydroxyapatite [NHA] from Waste Mussel Shells Using a Rapid Microwave Method. *Mater. Chem. Phys.* **2015**, *149*, 607–616. <https://doi.org/10.1016/j.matchemphys.2014.11.016>
- [58] Gayathri, B.; Muthukumarasamy, N.; Velauthapillai, D.; Santhosh, S.B. Magnesium Incorporated Hydroxyapatite Nanoparticles □: Preparation, Characterization, Antibacterial and Larvicidal Activity. *Arab. J. Chem.* **2018**, *11*, 645–654. <https://doi.org/10.1016/j.arabjc.2016.05.010>
- [59] Ruksudjarit, A.; Pengpat, K.; Rujijanagul, G.; Tunkasiri, T. Synthesis and Characterization of Nanocrystalline Hydroxyapatite from Natural Bovine Bone. *Curr. Appl. Phys.* **2008**, *8* (2-3), 270–272. <https://doi.org/10.1016/j.cap.2007.10.076>
- [60] Akhavan, A.; Sheikh, N.; Khoylou, F.; Naimian, F.; Ataeivarjovi, E. Synthesis of Antimicrobial Silver/Hydroxyapatite Nanocomposite by Gamma Irradiation. *Radiat. Phys. Chem.* **2014**, *98*, 46–50. <https://doi.org/10.1016/j.radphyschem.2014.01.004>
- [61] Feng, Q.L.; Wu, J.; Chen, G.Q.; Cui, F.Z.; Kim, T.N.; Kim, J.O. A Mechanistic Study of the Antibacterial Effect of Silver Ions on Escherichia Coli and Staphylococcus Aureus. *J. Biomed. Mater. Res.* **2000**, *52*, 662–668. [https://doi.org/10.1002/1097-4636\[20001215\]52:4<662::AID-JBM10>3.0.CO;2-3](https://doi.org/10.1002/1097-4636[20001215]52:4<662::AID-JBM10>3.0.CO;2-3)
- [62] Varkey, A.J. Antibacterial Properties of Some Metals and Alloys in Combating Coliforms in Contaminated Water. *Sci. Res. Essays.* **2010**, *5* (24), 3834–3839.

Received: August 12, 2021 / Revised: August 20, 2021 /
Accepted: September 28, 2021

ВИДЛЕННЯ АНТИБАКТЕРІАЛЬНОГО НАНО-ГІДРОКСИПАТИТНОГО БІОМАТЕРІАЛУ З КІСТОК БУЙВОЛІВ ТА ЙОГО ХАРАКТЕРИСТИКА

Анотація. *Методом термічного розкладу з біовідходів (кісток буйвола) виділені наночастинки гідроксиапатиту (НАр). Отриманий білий порошкоподібний матеріал охарактеризований за допомогою інфрачервоної спектроскопії з перетворенням Фур'є (FTIR), дифракції рентгенівських променів (XRD), скануючої електронної мікроскопії (SEM) та енергодисперсійного рентгенівського аналізу (EDX). За допомогою FTIR підтверджено, що термічне оброблення кісткового порошку при температурі 1223 К або вище видаляє органічні частини, що призводить до утворення чистого неорганічного біомінералу. Рентгенофазовий аналіз показав, що отриманий матеріал є нанокристалічним НАр (папо-НАр) із середнім діаметром зерен 25 нм, а їх паличкоподібні частинки з цілком агломерованою морфологією підтверджені аналізом SEM. Крім кальцію (Ca), фосфору (P) і кисню (O), слідові кількості алюмінію (Al), магнію (Mg), міді (Cu), цирконію (Zr) і вуглецю (C) виявлені за допомогою EDX. Антибактеріальну активність папо-НАр проти шести стандартних штамів досліджували методом дифузії. В інтервалі досліджуваних концентрацій встановлено, що найбільшу активність папо-НАр виявляє до Acinetobacter baumannii, меншу активність до Escherichia coli, Pseudomonas aeruginosa та Staphylococcus aureus, і зовсім неактивний щодо Salmonella typhi та Staphylococcus aureus, стійкого до метициліну (MRSA). Показано, що nano-НАр потенційно можна застосовувати в біомедицині.*

Ключові слова: кістки буйвола, гідроксиапатит, наноматеріал, антибактеріальна активність, біокераміка.